metals

MDPI

Article

Improvement of the Mechanical Properties of the Diffusion-Bonded 2024 Aluminum Alloy through Post-Weld Heat Treatments

Meng-Ting Chiang [1,2], Kuan-Yu Chiu [1,3], Po-Ching Wu [1], Shih-Ying Chang [4], Yu-Kai Sun [1,5] and Tung-Han Chuang [1,*]

[1] Department of Materials Science and Engineering, National Taiwan University, Taipei 10617, Taiwan
[2] United Microelectronics Co., UMC, Hsinchu 30078, Taiwan
[3] Delta Group Cyntec Co., Ltd., Hsinchu 30076, Taiwan
[4] Department of Mechanical Engineering, National Yunlin University of Science & Technology, Yunlin 64002, Taiwan
[5] Department of Power Mechanical Engineering, National Taitung Junior College, Taitung 95045, Taiwan
* Correspondence: tunghan@ntu.edu.tw; Tel.: +886-2-3366-1305

Abstract: In this study, 2024 aluminum alloy was diffusion bonded to identify the effect of the bonding temperature, applied pressure, and heating time on the microstructure, hardness, and bonding strength. The shear strength increased from 62.5 MPa to 81.2 MPa along with the rise in bonding temperatures from 440 °C to 490 °C. The bonding strength rose from 62.5 MPa to an optimal value of 81.2 MPa by extending the bonding time from 30 min to 240 min at a bonding temperature of 490 °C and a constant pressure of 5 MPa. In addition, various post-weld heat treatments for diffusion-bonded joints were also performed to improve the bond quality. After the T6 or T4 post-weld heat treatment, the hardness at the bonding interface and the substrate increased due to the precipitation of Al_2Cu. Post-weld T4 and T6 heat treatments increased the interface microhardness from 106.3 Hv to 138.25 Hv and 130.6 Hv, respectively. The bonding strength of the AA2024 was significantly improved up to 124.5 MPa and 164.3 MPa by the T4 and T6 heat treatments, respectively.

Keywords: diffusion bonding; post-weld heat treatments; 2024 aluminum alloy; microhardness; bonding strength

Citation: Chiang, M.-T.; Chiu, K.-Y.; Wu, P.-C.; Chang, S.-Y.; Sun, Y.-K.; Chuang, T.-H. Improvement of the Mechanical Properties of the Diffusion-Bonded 2024 Aluminum Alloy through Post-Weld Heat Treatments. *Metals* **2022**, *12*, 1738. https://doi.org/10.3390/met12101738

Academic Editor: Manuel Vieira

Received: 11 September 2022
Accepted: 14 October 2022
Published: 17 October 2022

1. Introduction

2024 aluminum alloy is a common feature in various industrial applications, such as aeronautics, aviation, automotive, and architecture, as a result of its high strength, light weight, good surface properties, and sufficient corrosion resistance [1]. An adequate bonding process to join similar or dissimilar materials is commonly required to enable the application of an aluminum alloy. Among the joining techniques for aluminum alloys, tungsten inert gas (TIG) welding, friction stir (FS) welding, laser welding, and brazing are used especially frequently for the manufacturing of aluminum products. However, the difficulties encountered in joining aluminum alloys by these methods remain to be resolved [2]. TIG welding is known to produce a large deformation, cause parent material fusion issues, be susceptible to porosity [3], and create a severe heat-affected zone. Investigations suggest that these problems easily cause failures in aluminum alloy workpieces [4]; moreover, the slow welding speed increases the production cost [5]. Apart from these issues, TIG welding does not offer operation under vacuum conditions [6], and the workpieces are bonded by docking rather than face-to-face bonding. Reactive metals usually do not heterogeneously bond by TIG welding [7].

As one of the alternatives to TIG welding, advanced FS welding mitigates some of the shortcomings of TIG welding, laser welding, and other types of fusion welding methods. Yet, this technology faces considerable problems, such as the formation of keyhole-induced

pores in the joint region [8]. As a result, the workpieces must be patched or mechanically repaired. Therefore, the workpieces need to be fixed very tightly during the FS welding process and are only able to connect horizontally [9]. In addition, the weld channel zone produces large unpredictable oxide films composed of onion rings and brittle intermetallic compounds, weakening the joints [10] and causing wear and deformation to the friction stirring tool [11]. Brazing, wherein metals are bonded together through the insertion of a filler metal with a melting point lower than that of aluminum alloy, has been popularly employed to bonded aluminum alloys. Brazing seems to be ideally suited for the joining of dissimilar metals and only requires a low process temperature; however, the AA2024 alloy has a low solidus temperature of 502 °C, making it difficult to braze with the conventional Al-12Si filler with a eutectic point of 577 °C.

Diffusion bonding is another type of solid-state joining method that allows the joining of metal workpieces through heating at a temperature below the melting point under adequate pressure. In contrast to the abovementioned bonding methods, diffusion bonding of aluminum alloys can be conducted without involving the liquid phase, and no additional filler metals are required. Diffusion-bonded joints usually most nearly resemble the mechanical and metallurgical properties of the parent metal, and the process has little contamination [12]. In a previous study by Burkhart et al., the diffusion-bonding technique was successfully applied to aerospace superplastic titanium alloy structures [13]. Bhatta et al. investigated the optimum conditions required for high-quality diffusion bonding to apply it to superplastic aluminum alloys [14]. Especially with the advent of the technology of aluminum alloys in high-tech industrial applications, more emphasis has been placed on developing high-quality welding methods for aluminum alloys. Diffusion bonding has a few inherent advantages over conventional welding due to its high welding capability, high flexibility, and low deformation, which does not involve any thermal cracking [15]. With great potential for modern power devices that require large exchange systems [16,17], diffusion-bonded joints with a large area range are becoming increasingly important to improve the reliability of heat-sensitive components in portable devices. However, diffusion bonding of aluminum alloys has always faced several challenges. Despite the high weldability properties of the alloy, it also faces limitations such as oxidation issues during bonding. Huang et al. used an organic surface coating to prevent the oxidation of superplastic 7075 aluminum alloy during diffusion bonding. The treated joints achieved an optimum shear strength of over 200 MPa, which was near that of the parent material [18].

Due to the melting point of aluminum at about 661 °C, the thermal stability of its alloy usually covers a temperature range substantially lower than other higher melting point materials. As a result, the property variation of aluminum alloys at elevated temperatures is highly influenced by their initial microstructure. Strength degradation related to grain growth can be severe in diffusion-bonded aluminum alloy joints due to the exposure to high process temperatures between 0.5 and 0.8 Tm (Tm = absolute melting temperature). To our knowledge, how the solid-state diffusion-bonding parameters affect the mechanical properties of homogenous AA2024 alloys has not been studied. Therein, the effects of post-weld heat treatments for AA2024 alloys after diffusion bonding were investigated and are presented in this study.

2. Materials and Methods

All the AA2024 plates used for diffusion bonding in this study had a size of 50 mm × 20 mm × 5 mm and were treated with T351 heat treatment (solid solution at 495 °C for 1 h, followed by subsequent natural aging). The chemical composition of AA2024 is listed in Table 1. Before the bonding process, the alloy plates were surface treated with 1000- and 2000-grit silicon carbide papers to reduce the surface scratches and enable the contact area for bonding. The surfaces were then rinsed with acetone to remove all possible oxide layers and contamination. Two lap joint configurations were used to evaluate the bonding strength and interfacial microstructure, as illustrated in Figure 1a,b, respectively. The contaminant-free surfaces were in reciprocating sliding contact and placed

on a hot press for bonding. The temperature ramp was set at 40 °C/min, and the heating was conducted in a 10^{-2} torr vacuum chamber. The specimens were heated at temperatures ranging from 440 °C to 490 °C for bonding periods of 30 to 240 min, constantly pressed under a pressure of 5 MPa. The post-weld heat treatments for the bonded specimens were heat treated with two different conditions, T4 (heated at 495 °C for 1 h and water quenched to room temperature) and T6 (similar to T4 and then aged at 191 °C for 12 h).

Table 1. The chemical composition (wt. %) of the AA2024 aluminum alloy.

Al	Cu	Mg	Mn	Si	Fe	Zn	Ti
Balance	4.61	1.41	0.5	0.05	0.12	0.15	0.02

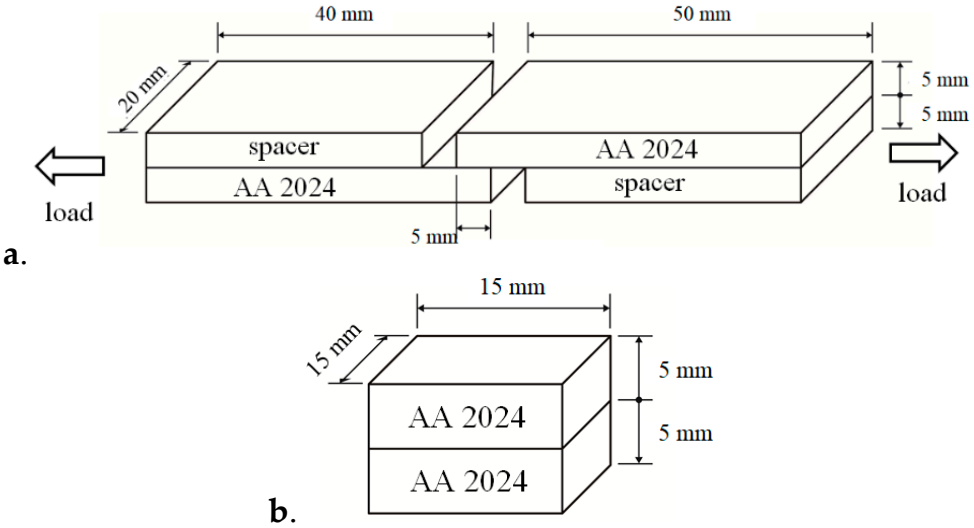

Figure 1. The geometry of the diffusion bonded AA2024 specimens for the shear tests (**a**) and microstructural observations (**b**).

For subsequent metallographic examination, the bonded samples were ground, polished, and etched by Keller's reagent to reveal the surface grain structure. The interfacial microstructures of the bonded specimens were then observed under a field-emission scanning electron microscope (FE-SEM, Nova Nano SEM 450, Thermo Fisher Scientific Inc., Waltham, MA, USA). Energy-dispersive X-ray (EDX) spectroscopy was applied to quantify the chemical composition of the precipitates formed at the bonding interface and the matrix. The shear strengths of the joints were determined with a tensile testing machine (Shimadzu AG-10TE, Kyoto, Japan) at a 1 mm/min crosshead speed at room temperature. At least three measurements of bonding shear strength were performed for each diffusion bonding condition, and the average was calculated. The fractography of both the diffusion-bonded and post-weld heat-treated AA2024 specimens were examined by metallographic observation with an FE-SEM with integrated EDX to identify the temperature effects on the overall microstructure at the joints.

The overall mechanical properties of the joints were further investigated by a microhardness tester at an indenting load of 100 gf and a dwell time of 10 s, in accordance with ASTM E384 standards [19]. The measurement position was at the center of the bonded specimen, with a hardness measurement of 0.1 mm intervals at each point horizontally extending to both sides from the center point, as indicated in Figure 2.

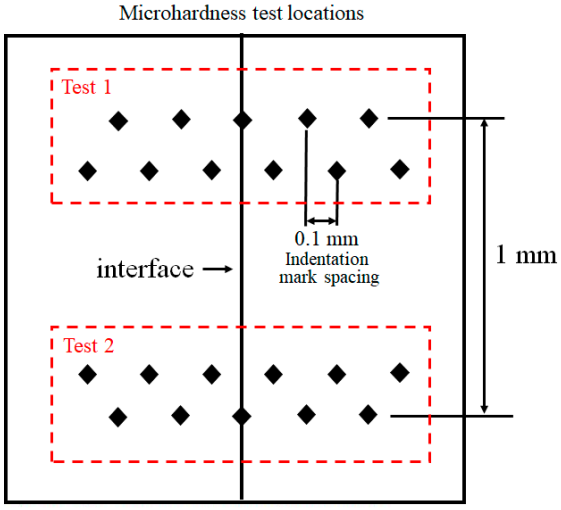

Figure 2. Microhardness measurement of the diffusion-bonded AA2024 specimens across the interface.

3. Results

The microstructure of the AA2024-T351 specimens before diffusion bonding (as-received) is shown in Figure 3. Precipitates appeared within the matrix of the alloy, as shown in Figure 3a. The compositions of the precipitates were about Al:Cu = 66.3:33.7 (at.%) and were identified as Al_2Cu intermetallic compounds by EDX spectrometry. The optical microscopy (OM), shown in Figure 3b, also revealed that the as-received AA2024-T351 specimens had an equiaxial grain distribution with an average size of about 75 μm.

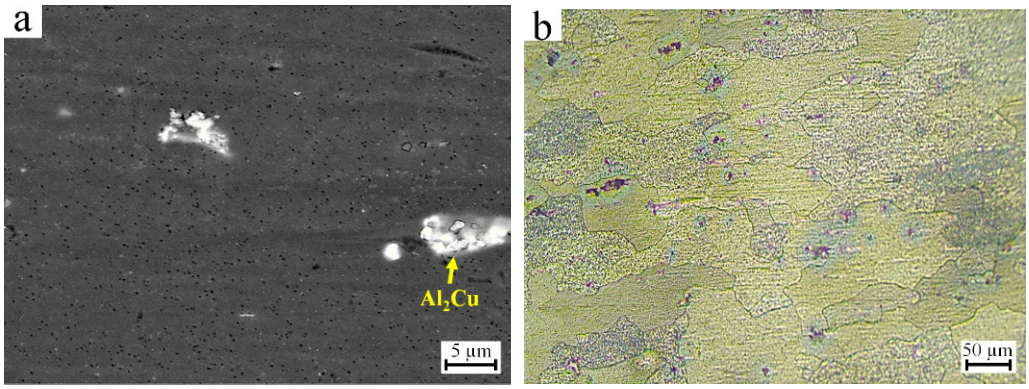

Figure 3. The SEM (**a**) and OM (**b**) images of the microstructure of the AA2024-T351 specimen before diffusion bonding.

The joint interfaces of the AA2024/AA2024 diffusion bonded at 490 °C under 5 MPa for different bonding periods are shown in Figure 4. After bonding for 30 min, voids started to appear at the interface, as shown in Figure 4a. The corresponding optical microscopy (OM) image in Figure 4e shows that the compressive stress of 5 MPa by the bonding process was sufficient to start to transform the original equiaxial coarse grains to slender grains. After extending the bonding periods from 30 min to 60 min, the voids at the interface disappeared, as shown in Figure 4b. However, a few slender precipitates began to form at the AA2024/AA2024 bonding interface after the diffusion-bonding process. After 120 min of bonding, the interfacial precipitates started to form coarse slender particles, as shown in Figure 4g. These slender grains within the AA2024 matrix grew with a prolonged bonding period. After 240 min of diffusion bonding at 490 °C, the coarse slender Al_2Cu precipitates remained at the void-free interface of the diffusion-bonded AA2024/AA2024 joint, as shown in Figure 4h. However, the slender grains in the AA2024 matrix recrystallized into

numerous approximately equiaxial grains with an average grain size of 32 µm, which was much finer than that of the as-received AA2024-T351 specimen before diffusion bonding.

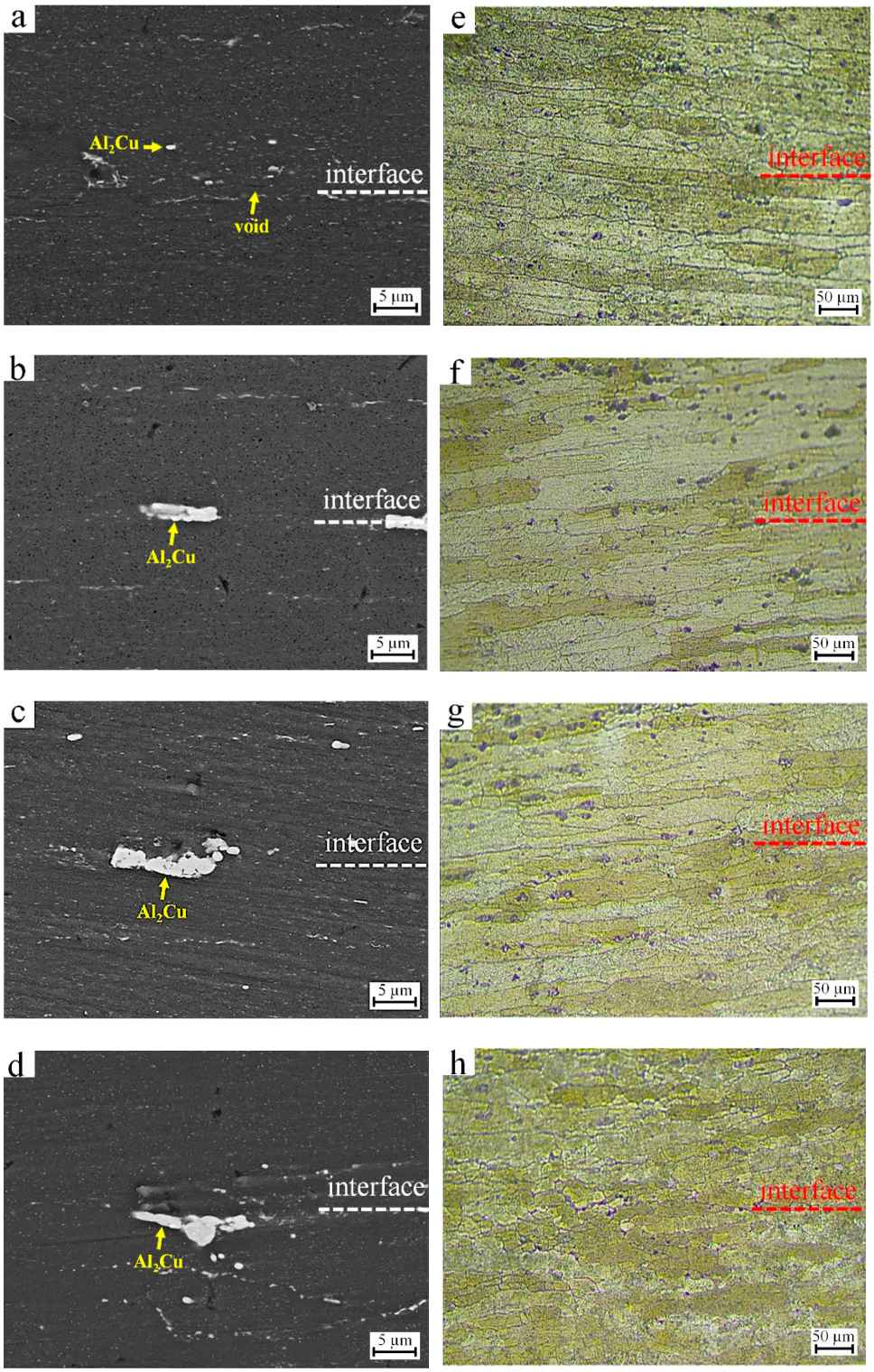

Figure 4. SEM images of the microstructure of the AA2024 specimen diffusion bonded at 490 °C for (**a**) 30 min, (**b**) 60 min, (**c**) 120 min, and (**d**) 240 min; (**e**–**h**) corresponding OM images.

The shear strength of the AA2024/AA2024 joints after diffusion bonding at 490 °C under the bonding pressure of 5 MPa is summarized in Figure 5. The shear strength increased from 62.5 MPa to 79.7 MPa by lengthening the bonding time from 30 min to

120 min.; it reached its maximum of 81.2 MPa at a bonding time of 240 min. On the other hand, decreasing the bonding temperature to 470 °C for 30 min of bonding resulted in a large drop in the shear strength from 62.5 MPa to 42.8 MPa. Although the bonding strength was improved to 68.7 MPa by extending the bonding period to 240 min, further decreasing the bonding temperature to 460 °C and 450 °C for 30 min continued to degrade the shear strength of the AA2024/AA2024 joints, to values of 41.3 MPa and 40.5 MPa, respectively. At lower temperatures, the shear strength was slightly improved by extending the bonding period. Diffusion bonding at 440 °C for 30 min resulted in a relatively low strength of 32.9 MPa. At this temperature, lengthening the bonding period to 240 min could not increase the shear strength as compared to the joints that were diffusion bonded at higher temperatures for a similar period of time.

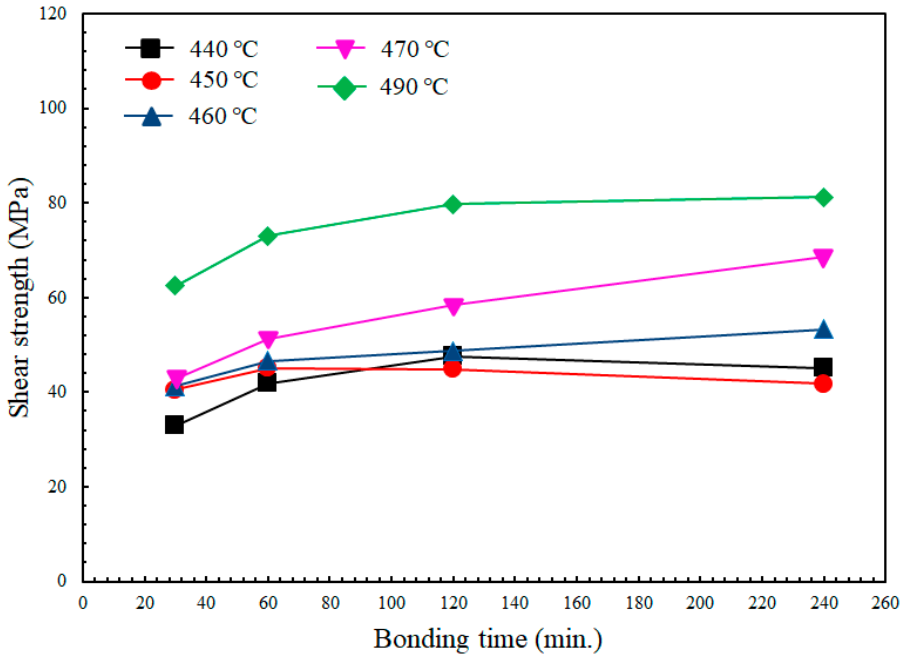

Figure 5. Shear strengths of the AA 2024/AA 2024 joints after diffusion bonding under 5 MPa for various bonding times and temperatures.

The AA2024/AA2024 joint diffusion bonded at 490 °C for 240 min. was further heat treated under the T4 and T6 conditions, respectively, to improve the bonding performance. Figure 6 shows that the T4 heat-treated (solid solution at 495 °C for 1 h and then water quenched) specimen exhibited an obvious improvement in shear strength, from 81.2 MPa to 125.1 MPa. Further aging at 191 °C for 12 h (T6 heat treatment) resulted in an optimum strength of 164.3 MPa, which was approximately 58% of the shear strength (283 MP) of the T6 heat-treated AA2024 alloy [20]. Saleh [21] diffusion bonded 2014 aluminum alloys using copper as an interlayer. The best tensile strength of 188.36 MPa was obtained under a joint pressure of 4 MPa at 475 °C. The study of Venugopal et. al. [22] pointed out that a higher bonding shear strength of diffusion bonded 5083 aluminum alloy could be obtained under higher temperatures and at higher bonding pressure. A shear strength of 119.46 MPa was obtained by diffusion bonding at 520 °C with a bonding pressure of 10 MPa for 30 min. The bonding strength of about 83–114 MPa was obtained in the study of Zinong et al. [23], who used a large-deformation hot-roll joining method to join 1060 aluminum alloy at a high temperature of 550–600 °C.

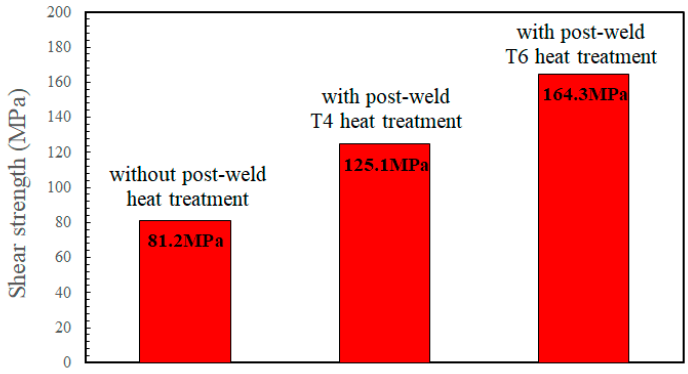

Figure 6. Shear strengths of the AA 2024/AA 2024 joints after diffusion bonding at 490 °C for 240 min and the post-weld T4 and T6 treatments.

The SEM images in Figure 7a,c and the OM images in Figure 7b,d reveal the microstructure of the AA2024/AA2024 joint after the post-weld T4 and T6 heat treatments. The slender coarse precipitates formed at the bonding interface in Figure 7b disappeared after the heat treatments and were replaced by larger grains (>150 μm) in the AA2024 matrix. Only a few voids were observed at the interface of the T4 heat-treated joint. Other than the obvious improvements in the bonding strength after the post-weld T4 and T6 heat treatments, the microhardness of the AA2024/AA2024 joints across the bonding interface was measured, as plotted in Figure 8b,c, which was higher than the hardness for the as-bonded AA2024/AA2024 joints (Figure 8a). For the T6 heat-treated AA2024/AA2024 joint, the measured microhardness was more or less the same as the T4 heat-treated AA2024/AA2024 joint. The microhardness at the interface after diffusion bonding was about 106.3 Hv at a bonding temperature of 490 °C for 240 min, which was similar to the hardness values of the substrate. After T4 heat treatment, the hardness at the interface increased to 138.3 Hv. The hardness in the substrate also increased to about the same hardness value. However, compared with the as-bonded or T4 heat-treated specimens, the difference between the two measured values of hardness after the T6 heat treatment was slightly larger, and the hardness distribution within the substrate was less uniform.

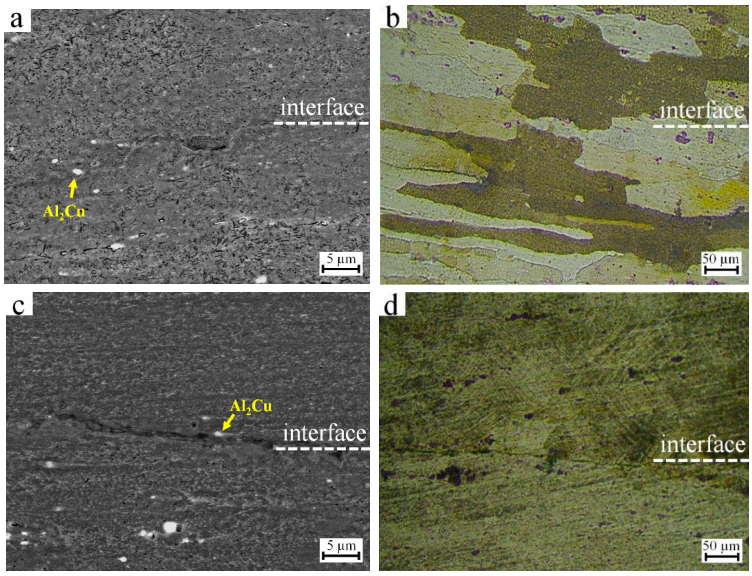

Figure 7. The SEM (**a**,**c**) and OM (**b**,**d**) images of the interfacial microstructure of the diffusion-bonded AA2024/AA2024 joints after the T4 (**a**,**b**) and T6 (**c**,**d**) heat treatments.

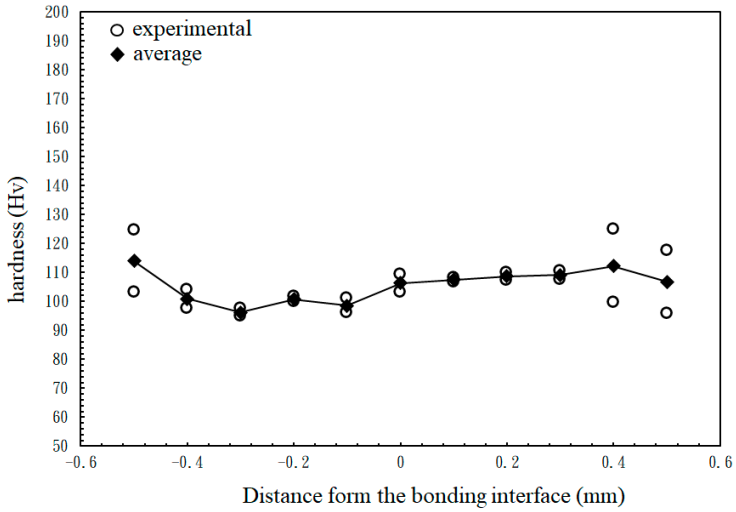

(**a**).

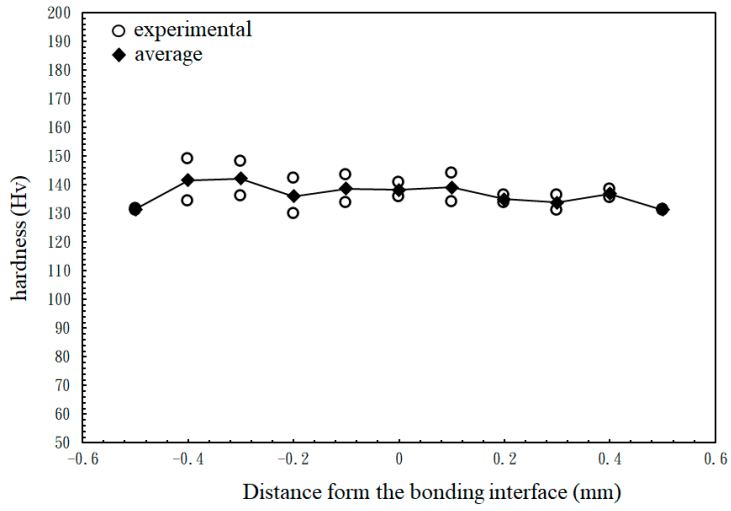

(**b**).

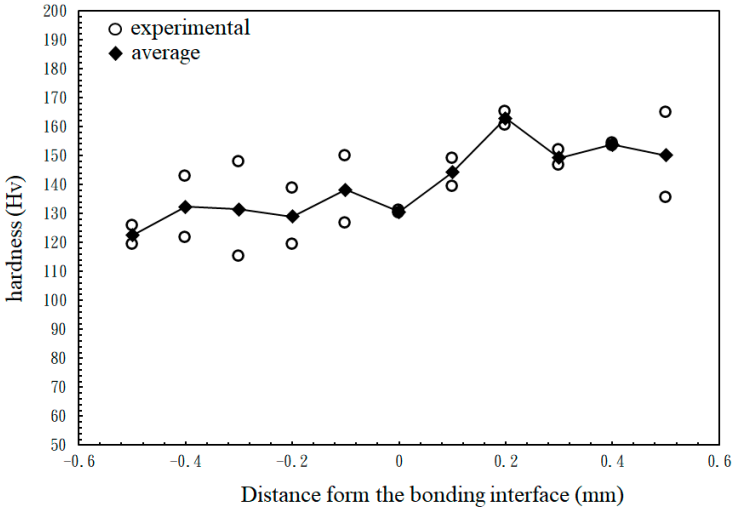

(**c**).

Figure 8. Microhardness measurements across the bonding interface of the AA2024/AA2024 joints: (**a**) as-bonded, (**b**) T4 heat treated, and (**c**) T6 heat treated.

The doubling of the shear strength from 81.2 MPa to 164.3 MPa after the T6 heat treatment for the AA2024/AA2024 joint compared with the as-bonded AA2024/AA2024

joint diffusion bonded at 490 °C for 240 min was attributed to the precipitation hardening of the AA2024 matrix due to the aging effect of the T6 heat treatment, which was consistent with the microhardness measurements of the specimens. As shown in Figure 8c, the microhardness of the AA2024/AA2024 joint reached its maximum value at approximately 160 Hv after the T6 heat treatment at 191 °C for 12 h.

The fractured surfaces after the shear tests for the AA2024/AA2024 joints before and after the post-weld heat treatments are shown in Figure 9. Both the as-bonded and the post-weld heat-treated specimens fractured along the bonding interfaces. Figure 9a shows an obvious shear band characteristic in the fractography of the as-bonded AA2024/AA2024 joint. The appearance of such a shear band structure on the fracture surface of the as-bonded AA2024/AA2024 joints can be correlated with the softening effect of the precipitation-free zone near the slender coarse Al_2Cu precipitates grown at the bonding interface. The existence of these coarse precipitates can cause severe crack issues along the interface, leading to local peeling at the joints. In contrast, the post-weld T4 and T6 heat treatments caused the formation of dimple structures in the AA2024/AA2024 joints, as shown in Figure 9b,c. The T4 and T6 post-weld heat treatments significantly improved the mechanical properties of the diffusion bonded AA2024/AA2024 joints by the dissolution of the slender coarse Al_2Cu precipitates formed at the as-bonded interfaces. Furthermore, the aging process of T6 heat treatment created precipitates in the AA2024/AA2024 matrix, contributing a strengthening effect to the overall microstructure of the AA2024/AA2024 joints. Combining the dissolution effect and the precipitation hardening of the AA2024 matrix by the post-weld T6 heat treatment, the shear strength of the joint was successfully optimized up to 164.3 MPa.

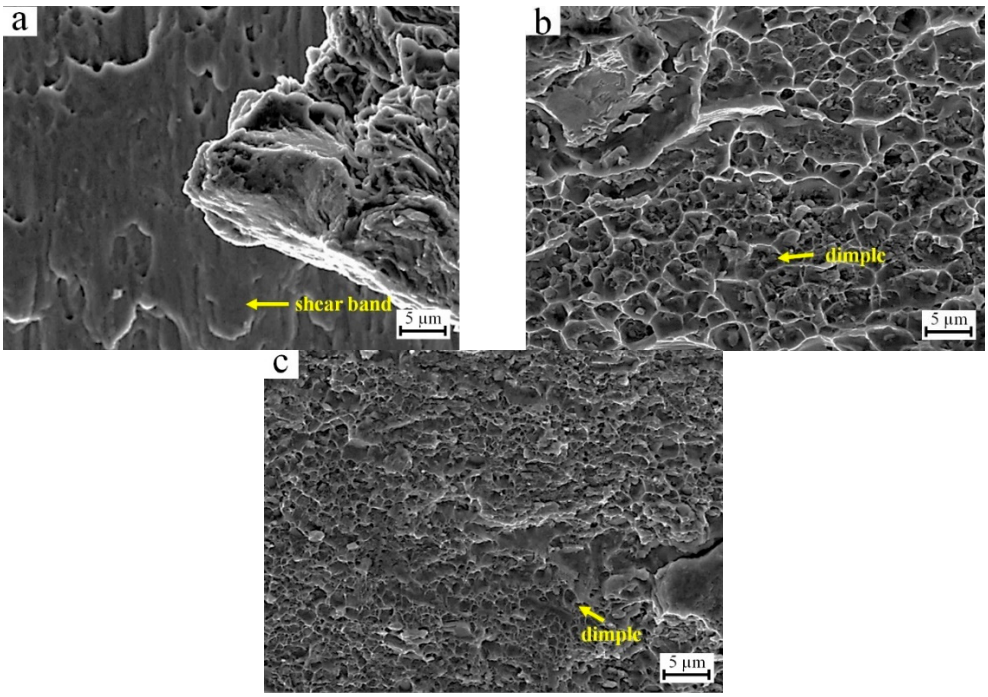

Figure 9. Fractography of the diffusion bonded AA2024/AA2024 joints after the shear tests: (**a**) as-bonded, (**b**) T4 heat treated, and (**c**) T6 heat treated.

4. Conclusions

The relationship between the joint microstructure and the shear strength was investigated for both diffusion-bonded AA2024/AA2024 joints before and after post-weld heat treatments. Diffusion bonding at 440 °C for 30 min resulted in a relatively low strength of 32.9 MPa. A higher bonding shear strength was obtained at higher temperatures and longer bonding periods. The shear strength of the joint increased from 62.5 MPa to 81.2 MPa by lengthening the bonding time from 30 min to 240 min at a bonding temperature of 490 °C.

Slender coarse Al_2Cu precipitates grew along the bonding interfaces accompanying the voids' annihilation during the diffusion bonding. The post-weld heat treatments T4 and T6 dissolved these undesired slender coarse precipitates and increased the overall microhardness of the bonding interfaces and the substrates and shear strength of the AA2024/AA2024 joints. Additional precipitation hardening during the aging process of the T6 heat treatment further improved the shear strength to 164.3 MPa, above double that of the as-bonded AA2024/AA2024 joint at a bonding temperature of 490 °C for 240 min.

Author Contributions: Conceptualization, M.-T.C., K.-Y.C., Y.-K.S. and T.-H.C.; data curation, M.-T.C., K.-Y.C., P.-C.W. and Y.-K.S.; investigation, M.-T.C., K.-Y.C., P.-C.W. and Y.-K.S.; methodology, M.-T.C. and Y.-K.S.; writing—original draft, M.-T.C., K.-Y.C., P.-C.W., S.-Y.C., Y.-K.S. and T.-H.C.; writing—review and editing, S.-Y.C., Y.-K.S. and T.-H.C.; supervision, T.-H.C.; project administration, T.-H.C. All authors have read and agreed to the published version of the manuscript.

Funding: This study was sponsored by the industrial and academic cooperation program of Plus Metal Tech., Co., Ltd., Tainan, Taiwan and the Ministry of Science and Technology, Taiwan, under Grant No. MOST 109-2622-E-002-030-CC2.This research received no external funding.

Institutional Review Board Statement: Not applicable.

Informed Consent Statement: Not applicable.

Data Availability Statement: Not applicable.

Conflicts of Interest: The authors declare no conflict of interest.

References

1. Kuhlmann, A.M. The second most abundant element in the earth's crust. *JOM* **1963**, *15*, 502–505. [CrossRef]
2. Abd El-Hameed, A.M.; Abdel-Aziz, Y.A. Aluminium Alloys in Space Applications: A Short Report. *J. Appl. Sci. Eng.* **2021**, *22*, 1–7. [CrossRef]
3. Deepati, A.K.; Alhazmi, W.; Benjeer, I. Mechanical characterization of AA5083 aluminum alloy welded using resistance spot welding for the lightweight automobile body fabrication. *Mater. Today Proc.* **2021**, *45*, 5139–5148. [CrossRef]
4. Çevik, B.; Koç, M. The effects of welding speed on the microstructure and mechanical properties of marine-grade aluminium (AA5754) alloy joined using MIG welding. *Kov. Mater* **2019**, *57*, 307–316.
5. Koprivica, A.; Bajić, D.; Šibalić, N.; Vukčević, M. Analysis of welding of aluminium alloy AA6082-T6 by TIG, MIG and FSW processes from technological and economic aspect. *Mach. Technol. Mater.* **2020**, *14*, 194–198.
6. Tung, S.K.; Lim, L.C. Void formation in wide gap brazing using prepacks of nickel base braze mixes. *J. Mater. Sci. Technol.* **1994**, *10*, 364–369. [CrossRef]
7. Liu, T.T.; Song, B.; Huang, G.S.; Jiang, X.Q.; Guo, S.F.; Zhang, K.H.; Pan, F.S. Preparation, structure and properties of Mg/Al laminated metal composites fabricated by roll-bonding, a review. *J. Magnesium Alloys.* **2022**, *10*, 2062–2093. [CrossRef]
8. Choudhary, A.K.; Jain, R. Fundamentals of Friction Stir Welding, Its Application, and Advancements. In *Welding Technology*; Springer: Cham, Switzerland, 2021; pp. 41–90.
9. Heidarzadeh, A.; Mironov, S.; Kaibyshev, R.; Çam, G.; Simar, A.; Gerlich, A.; Khodabakhshi, F.; Mostafaei, A.; Field, D.P.; Robson, J.D.; et al. Friction stir welding/processing of metals and alloys: A comprehensive review on microstructural evolution. *Prog. Mater. Sci.* **2021**, *117*, 100752. [CrossRef]
10. Bang, H.S.; Hong, S.M.; Das, A.; Bang, H.S. Study on the weldability and mechanical characteristics of dissimilar materials (Al5052-DP590) by TIG assisted hybrid friction stir welding. *Met. Mater. Int.* **2021**, *27*, 1193–1204. [CrossRef]
11. Majeed, T.; Mehta, Y.; Siddiquee, A.N. Analysis of tool wear and deformation in friction stir welding of unequal thickness dissimilar Al alloys. *Proc. Inst. Mech. Eng. L* **2021**, *235*, 501–512. [CrossRef]
12. Peng, L.; Yajiang, L.; Haoran, G.; Juan, W. Investigation of interfacial structure of Mg/Al vacuum diffusion-bonded joint. *Vacuum* **2006**, *80*, 395–399. [CrossRef]
13. Burkhart, E.T.; Hefti, L. Advancements of Superplastic Forming and Diffusion Bonding of Titanium Alloys for Heat Critical Aerospace. *SAE Tech. Pap.* **2020**, *2*, 1202–1208.
14. Bhatta, L.; Pesin, A.; Zhilyaev, A.P.; Tandon, P.; Kong, C.; Yu, H. Recent development of superplasticity in aluminum alloys: A review. *Metals* **2020**, *10*, 77. [CrossRef]
15. Sajan, M.; Sampatirao, H.; Balasubramanian, R.; Nagumothu, R. Plasma electrolytic oxidation of AZ31 magnesium alloy diffusion bonded with aluminium. *Mater. Today Proc.* **2021**, *46*, 972–976. [CrossRef]
16. AlHazaa, A.; Haneklaus, N.; Almutairi, Z. Impulse pressure-assisted diffusion bonding (IPADB): Review and outlook. *Metals* **2021**, *11*, 323. [CrossRef]
17. Shioga, T.; Mizuno, Y.; Nagano, H. Operating characteristics of a new ultra-thin loop heat pipe. *Int. J. Heat Mass Transf.* **2020**, *151*, 119436. [CrossRef]

18. Huang, Y.; Ridley, N.; Humphrey, F.J.; Cui, J.Z. Diffusion bonding of superplastic 7075 aluminum alloy. *Mater. Sci. Eng. A* **1999**, *266*, 295–302. [CrossRef]
19. *ASTM-E384*; Test Method for Microindentation Hardness of Materials. ASTM International: West Conshohocken, PA, USA, 2017.
20. ASM Aerospace Specification Metals Inc.: Pompano Beach, FL, USA, 2001. Available online: https://asm.matweb.com/search/SpecificMaterial.asp?bassnum=ma2024t6 (accessed on 9 September 2022).
21. Saleh, A.A. Microstructure and strength of diffusion bonded 2014 AA alloys using copper interlayer. *Open J. Appl. Sci.* **2019**, *9*, 342–353. [CrossRef]
22. Venugopal, S.; Seeman, M.; Seetharaman, R.; Jayaseelan, V. The effect of bonding process parameters on the microstructure and mechanical properties of AA5083 diffusion-bonded joints. *Int. J. Ligh. Mater. Manuf.* **2022**, *5*, 555–563. [CrossRef]
23. Zinong, T.; Bing, Z.; Jun, J.; Zhiqiang, L.; Jianguo, L. A study on the hot roll bonding of aluminum alloys. *Proc. Manuf.* **2020**, *50*, 56–62. [CrossRef]